Modul B.Phy.407.Mp: Einführung ins wissenschaftliche Arbeiten

Particle simulations of polymer mixtures in confined geometries with time dependent boundary conditions

prepared by

Justus Multhaup

from Boffzen

at the Institut für Theoretische Physik

Contents

1 Introduction

Polymers are highly versatile macromolecules composed of repeating units called monomers. Their importance for life on earth cannot be overstated, biological polymers are involved in countless chemical reactions in the human body and form the backbone of proteins and DNA. Synthetic polymers are applied almost everywhere in modern society, ranging from simple packaging materials to highly sophisticated materials used in aerospace engineering. This is owed to their vast range of unique physical properties, such as high elasticity, flexibility and durability. When creating novel materials with very precise features, understanding how polymers interact with one another and form structure via phase separation in multipcomponent systems is essential.

One important class of polymers is the so-called homopolymer, which is made of a single type of monomer unit, for example, polyethylene. Copolymers, in contrast, consist of two or more different types of monomer units. Copolymers that are concatenations of homopolymers of different types and lengths are called block-copolymers. One of the most interesting and extensively studied properties of copolymers is their ability to self-assemble into microphases [11]. An important tool in understanding the mechanisms behind this microphase separation, and many other interesting properties, is the use of computer simulations. These include particle-based molecular dynamics (MD) and Monte-Carlo (MC) methods as well as continuum-model-based and hybrid methods [16]. Particle-based simulations accurately model small-scale phenomena. However, despite rapid advancements in computer technology and high parallelizability, they are too computationally expensive to simulate long time scales since they involve the explicit calculation of the strong, bonded interactions between particles. This also poses limitations on the system size; macro scale phenomena are hard to capture. Continuum models, on the other hand, are less computationally expensive, but at the cost of a lower accuracy on the microscale. On the mesoscale, good agreement between the two types of models was observed, e.g. in the orientation of cylindrical mesophases upon sol-

vent evaporation [6]. To evaluate the accuracy of continuum models on small-length scales, it is necessary to compare them to established particle-based models. One approach to this is to consider a simulation box in a particle-based simulation as a small section from a large continuum-model-based simulation. The dynamics are then driven by extracting the time evolution of the density fields at the boundaries from the continuum simulation and applying them in the particle-based simulation, e.g. employing non-periodic boundary conditions. However, dictating the boundary densities in particle-based simulations is not a trivial task. One option is the use of external fields or the umbrella sampling method [23], although this has the large drawback that the number of particles in the simulation box remains constant, while in the continuum simulation particles can enter and leave the section at any time. An alternative is to employ conversion zones at the boundaries, in which molecules are converted to different types, mimicking particle exchange with the surrounding as shown in Figure 1.1. If the densities are defined on a discretized grid, this leads to an optimization problem in which the ideal configuration of molecule types needs to be found, such that the mean squared deviation from the target density is minimized.

In this study, as a first step towards boundary-driven particle simulations, the dynamics of noninteracting homopolymers are investigated. Specifically, a system is pushed away from equilibrium by introducing conversion zones at the boundary regions of the simulation box. This results in a diffusive current and allows the calculation of the collective diffusion coefficient of the system. To this end, the SOft coarse-grained Monte-Carlo Acceleration (SOMA) [20] software package based on the single chain in mean field algorithm (SCMF) [4] is employed.
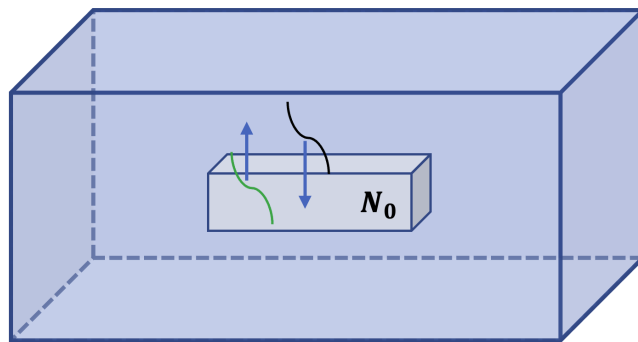

Figure 1.1: Sketch of the setting explained in the text. Polymers of different types may be exchanged with the surrounding, but the number of molecules N_0 inside the section of the particle simulation remains constant.

2 Theory

2.1 Single-chain properties

Since the collective dynamics of polymer mixtures can often be directly related to the single-chain properties, some selected aspects are briefly discussed here. The simplest model to describe a polymer chain is the ideal chain, for which any non-bonded interaction between monomers is neglected.

2.1.1 The freely jointed chain

The freely jointed chain model is an ideal model in which the chain is composed of N segments of length a, whose orientation vectors $\mathbf{r}_i$ ($a = |\mathbf{r}_i|$) can face in any direction and are completely independent from each other. The chain configuration may be characterised by the *end-to-end-vector* $\mathbf{R}$:

$$\mathbf{R} = \sum_{i=1}^{N} \mathbf{r}_i \,. \tag{2.1}$$

Due to the completely random orientation, $\mathbf{R}$ has zero mean. A useful property to quantify the spatial extension of the chain is the mean square of $\mathbf{R}$, which calculates to:

$$R_e^2 \equiv \langle \mathbf{R}^2 \rangle = N a^2 \,. \tag{2.2}$$

For large N, $\mathbf{R}$ has a Gaussian distribution [12]:

$$P(N, \mathbf{R}) = \left(\frac{3}{2\pi R_e^2} \right)^{3/2} \exp\left[-\frac{3\mathbf{R}^2}{2R_e^2} \right] \,, \tag{2.3}$$

the freely jointed chain therefore converges towards the Gaussian chain.

2.1.2 Rouse model

The Rouse model [19] is used to describe the dynamics of a Gaussian chain moving through a solvent. The stiff bonds are replaced by springs of root-mean-square size b, through which a monomer interacts with its neighbours. The monomers experience a friction force with friction coefficient ζ, the total friction coefficient of the center of mass is:

$$\zeta_\mathrm{R} = N\zeta \,.$$

(2.4)

Within the Rouse model, the diffusion coefficient of the chain is computed as:

$$D_\mathrm{R} = \frac{k_B T}{\zeta_\mathrm{R}} = \frac{k_B T}{N\zeta} \,.$$

(2.5)

The time in which a polymer diffuses a distance of the order of its size is called relaxation time τ_R:

$$\tau_\mathrm{R} \approx \frac{R_e^2}{D_\mathrm{R}} = \frac{\zeta}{k_B T} N R_e^2 \,.$$

(2.6)

On time scales larger than τ_R, the chain movement is only due to diffusion, while viscoelastic effects are observed at shorter time scales.

2.2 Polymeric mixtures

Polymer mixtures consist of two or more chemically different polymer types. The mechanical and thermodynamic properties can vary greatly with several factors such as composition, molecular weight and interactions between the polymers. This makes them desirable for manufacturing materials with tailored properties.

If the composition is uniform everywhere, the mixture is called homogeneous. In a heterogeneous mixture, in contrast, the composition is non-uniform, leading to visible boundaries which may have very different properties. This phenomenon is

also called macro-phase separation. From an entropic viewpoint, mixing is always favored. However, energetic interactions between polymers may either favor or suppress mixing. Whether a mixture is homogeneous or heterogeneous, thus, depends on the balance between entropy and energy [12, S. 137].

2.2.1 Flory-Huggins Theory

Whether mixing or phase separation will be favored can be predicted by determining the free-energy change associated with mixing the components. This free energy-change can be computed within the lattice model developed by Flory and Huggins [9]. Within the Flory-Huggins framework, no volume change is assumed upon mixing. With this assumption, it is convenient to represent the system on a lattice. A lattice site corresponds to the smallest molecular unit and every macromolecule takes up one or multiple lattice sites. Consider a binary mixture with n_A polymers of species A and chain length N_A and n_B polymers of species B and chain length N_B. Let the total number of polymers be $n = n_A + n_B$. The free energy of mixing per monomer ΔF_{mix} is then given by the Flory-Huggins equation of polymer solutions [12, S. 143]:

$$\frac{\Delta F_{mix}}{k_B T} = \frac{\phi}{N_A} \ln \phi + \frac{1 - \phi}{N_B} \ln(1 - \phi) + \chi \phi (1 - \phi) \,. \tag{2.7}$$

Here, $\phi = n_A N_A / (n_A N_A + n_B N_B)$ is the monomer fraction of species A, k_B is the Boltzmann constant, T is the system temperature and χ is the Flory interaction parameter which characterizes the interaction between different polymer species and can be obtained from experiments. A positive value of χ opposes mixing while a negative value promotes it; knowing the value of χ, therefore, allows us to qualitatively predict the phase separation behavior. For $\chi = 0$, (2.7) reduces to regular solution theory for an ideal gas of polymers with concentrations ϕ/N_A and $(1 - \phi)/N_B$. Note that so far, no space dependency of ϕ has been assumed. In the following discussion, a symmetric mixture with $N_A = N_B = N$ is assumed. To fully capture the complexity of the system, the Flory-Huggins model has to be extended to include spatial variations of ϕ, which gives rise to the de Gennes-Flory-Huggins free-energy functional [5, 17]:

$$\frac{F[\phi]R_e^3}{k_B T \sqrt{\bar{N}}} = \int \mathrm{d}^3\mathbf{r} \left\{ \phi \ln \phi + (1-\phi)\ln(1-\phi) + \chi N \phi(1-\phi) + k(\phi)[\nabla \phi]^2 \right\} . \quad (2.8)$$

Here, $\bar{N} = (nR_e^3/V)^2$ is the invariant degree of polymerization of the system with volume V. It is a measure of the number of neighboring chains a chain interacts with. The term proportional to $[\nabla \phi]^2$ is added to the free-energy density to ensure that unphysical, sharp changes in the local densities are penalized. The precise form of $k(\phi)$ depends on the strength of the parameter χ. For small $\chi N \lesssim 5$, one considers the *weak segregation limit* (WSL). For large $\chi N \gtrsim 10$ [21], the *strong segregation limit* (SSL) holds. In these two limits, the prefactor k takes the following form [17]:

$$k_{\mathrm{WSL}} = \frac{R_e^2}{36\phi(1-\phi)} ; \qquad k_{\mathrm{SSL}} = \frac{R_e^2}{24\phi(1-\phi)} . \quad (2.9)$$

2.3 Collective diffusion

Consider again a binary mixture of polymers with $N_A = N_B = N$. Since the number of polymers in the system is constant, the continuity equation holds:

$$\frac{\partial \phi}{\partial t} + \nabla \cdot \mathbf{J}_A = 0 . \quad (2.10)$$

Here, $\mathbf{J}_A$ is the local current of polymer species A. Near equilibrium, one postulates a linear relation between $\mathbf{J}_A$ and the local chemical potential μ_A [5]. In the most general case, this relation is non-local in space and time. Assuming translational invariance in space and time, it reads [8]:

$$\mathbf{J}_A(\mathbf{r}, t) = -\int_{t'=-\infty}^{t} \mathrm{d}t' \int_V \mathrm{d}\mathbf{r}' \frac{\Lambda_A(\mathbf{r}-\mathbf{r}', t-t')}{k_B T} \nabla' \mu_A(\mathbf{r}', t') . \quad (2.11)$$

The Onsager coefficient $\Lambda_A(\mathbf{r}-\mathbf{r}', t-t')$ relates the gradient of the chemical potential at position $\mathbf{r}'$ to a density flux at position $\mathbf{r}$ and also accounts for memory effects. The non-localities in (2.11) translate into a dependency of Λ on the wave vector $\mathbf{q}$ and the frequency ω in Fourier space. In the time-independent steady state, this gives:

$$\mathbf{J}_{\mathrm{A},q} = -iq\frac{\Lambda_{\mathrm{A},q}}{k_B T}\mu_{\mathrm{A},q}\,, \tag{2.12}$$

where $q = |\mathbf{q}|$. In the following, it is assumed that $\mu[\phi(x)] \propto x$, so $\mu_q \propto 1/q$ and $\nabla\mu = \mathrm{const}$. For a spatially independent current, this implies that Λ must also be independent of q, so in the spatial picture:

$$\mathbf{J}_{\mathrm{A}} = -\frac{\Lambda_{\mathrm{A}}}{k_B T}\nabla\mu_{\mathrm{A}}\,. \tag{2.13}$$

This approximation holds for small q and therefore prohibits the probing of the q-dependence of Λ, but it leads to a simple form of the Onsager coefficient that will be derived in the following.

Following the discussion in the appendix of [5], consider a mixture of polymer chains with densities ϕ_{A} and ϕ_{B}. Incompressibility, e.g. $\phi_{\mathrm{A}} + \phi_{\mathrm{B}} = 1$, is enforced by introducing an additional repulsive potential U to the chemical potential, so from (2.13) one obtains:

$$\mathbf{J}_{\mathrm{A}} = -\Lambda_{\mathrm{A}}\nabla[(\mu_{\mathrm{A}} + U)/k_B T]\,, \tag{2.14a}$$

$$\mathbf{J}_{\mathbf{B}} = -\Lambda_{\mathrm{B}}\nabla[(\mu_{\mathrm{B}} + U)/k_B T]\,. \tag{2.14b}$$

Due to the incompressibility, the total current $\mathbf{J} = \mathbf{J}_{\mathrm{A}} + \mathbf{J}_{\mathrm{B}}$ must have zero divergence, which in one dimension means $\mathbf{J} \equiv J\mathbf{e_x} = \mathrm{const}$. From the Galilei invariance of the system, we can simply choose $J = 0$. From this condition, U can be calculated explicitly:

$$U = (\Lambda_{\mathrm{A}}\mu_{\mathrm{A}} + \Lambda_{\mathrm{B}}\mu_{\mathrm{B}})/(\Lambda_{\mathrm{A}} + \Lambda_{\mathrm{B}})\,. \tag{2.15}$$

Since one of the currents is redundant, write $J \equiv J_A$. From (2.14), obtain:

$$J = -\Lambda\nabla(\mu_{\mathrm{A}} - \mu_{\mathrm{B}}) \equiv -\Lambda\nabla\mu\,, \tag{2.16}$$

where $\Lambda = \Lambda_A \Lambda_B/(\Lambda_A + \Lambda_B)$ and μ is the exchange chemical potential. In the limit of no interactions, the mixture can be considered as an ideal gas, so $\Lambda_i = D_i/\phi_i$ for $i = A, B$. For $D_A = D_B \equiv D$, this yields:

$$\Lambda = D\phi(\mathbf{r})(1 - \phi(\mathbf{r})). \qquad (2.17)$$

This approximation is frequently used in the literature for the sake of computational efficiency [3, 5, 10]. It corresponds to a local coupling in which monomers move like the center of mass, therefore it does not account for the connectivity of the monomers along the backbone of the chain.

3 Simulation technique

To simulate the collective dynamics, a coarse-grained model of the polymers is employed. Within this model, several monomeric repeat units are grouped into an effective interaction center, called *bead*, which allows for an efficient numerical implementation. Nevertheless, in this study, the terms "bead" and "monomer" will be used interchangeably. A great variety of universal properties of polymeric materials on mesoscopic length scales is accurately captured by coarse-grained models [1].

The software package that is used for the numerical calculations, SOft coarse-grained Monte-Carlo Acceleration (SOMA) [20], uses a combination of a coarse-grained model and the single-chain-in-mean field-algorithm (SCMF) [4]. Unlike the widely used self-consistent-field theory (SCF), the SCMF method includes fluctuation effects which are required to accurately describe certain systems and effects, e.g. dilute polymer solutions, the vicinity of phase transitions, or polymeric microemulsions [2, 7, 13]. Instead of calculating the interaction of a chain with all its surrounding explicitly, the chains are subjected to fluctuating external fields which are frequently recalculated from the density distribution. The densities are defined on a cubic grid. The time evolution of the system is then performed by MC simulation and the external fields remain constant during one MC sweep, this is called *quasi-instantaneous field approximation.* The enormous benefit of this is that the chains are decoupled, making it possible to implement it effectively on parallel machines and leverage accelerators like Nivida GPUs [20]. Additionally, a Smart Monte-Carlo (SMC) scheme is employed that uses the strong bonded forces to propose a trial displacement resembling Brownian motion and produces Rouse-like dynamics [15, 18].

While a full description of the SCMF equations can be found in [4], and will be omitted here, it is important to note that the interactions are fully described by three coarse-grained parameters: the average mean squared end-to-end distance R_e^2 of a chain in the absence of non-bonded interactions, the inverse thermal compressibility $\kappa_o N$ and the incompatibility between different bead types $\chi_o N$. The term "soft" in SOMA relates to the soft nature of the non-bonded interactions, which arises from

the systematic coarse-graining and allows for an overlap of beads [14].

4 Collective diffusion of symmetric homopolymers

4.1 Reference system

In this section, the collective diffusion properties of noninteracting homopolymers with $N_A = N_B = N$ and $\chi = 0$ are investigated. As a reference system, a simulation box with $n = 10000$ polymers and dimensions $L_x \times L_y \times L_z = 9.75 \times 3 \times 3\,R_e^3$ is used, so the invariant degree of polymerization is $\sqrt{\overline{N}} \approx 114$. The spatial discretization is $\Delta L = 0.125\,R_e$. Periodic boundary conditions are applied in the lateral y and z directions, whereas impenetrable walls are applied in the x direction. Initially, the polymers are distributed homogeneously in the system. To stimulate a flux in a non-equilibrium steady state (NESS), conversion zones of width $d = 0.25\,R_e$ are introduced close to the walls. In each time step, if the center-of-mass coordinate $\mathbf{r}_{cm}$ of a polymer of type A lies in the left conversion zone, it is converted to type B with probability $p(A \to B) = r$. Analogously, conversion from B to A takes place in the right conversion zone with the same probability r. The current $\mathbf{J}$ is measured by tracking the number of polymer conversions. The simulation setup is depicted in Figure 4.1.

The computation of the transport properties is complicated by boundary effects, such as a steep density drop close to the hard walls, which is of entropic origin. Furthermore, chains whose center of mass lies in the conversion zone may extend far beyond that zone. The range of these effects is approximated as R_e and measurements are only taken in the region where the effects are negligible.

4.2 Collective diffusion coefficient

Due to the periodic boundary conditions and the spatial homogeneity in the lateral directions, the system can effectively be described in one dimension. The density
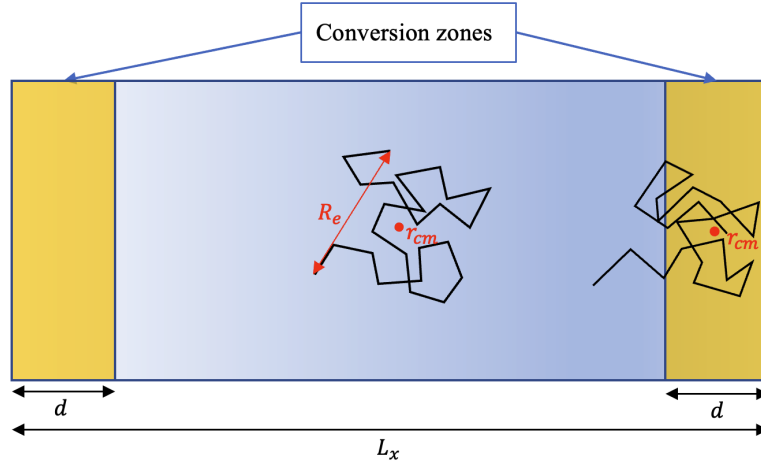
Figure 4.1: Simulation setup. For clarity, the conversion zones are not to scale and no distinction between polymer types is made.
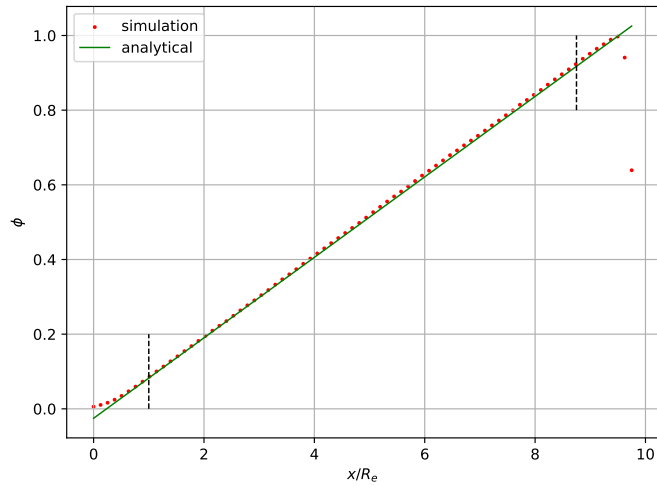
profile for $r = 1.0$ is shown in Figure 4.2.

Figure 4.2: Steady-state density profile for $r = 1.0$ averaged over y and z. The analytical curve corresponds to (4.4). The black lines mark the region that is estimated to be affected by boundary effects.

Outside of the range of the boundary effects, the density profile is very well represented by a linear function. The chemical potential is obtained by taking the functional derivative $\frac{\delta F}{\delta \phi}$ of (2.8). Since $\chi = 0$, no phase separation occurs and the local density differences are entirely due to the dynamics. Assuming the WSL, the chemical potential becomes:

$$\frac{\mu R_e^3}{\sqrt{\bar{N}}k_B T} = \ln \phi - \ln(1 - \phi) - \frac{R_e^2}{18\phi(1 - \phi)}\phi''$$

$$+ \left[\frac{R_e^2(1 - 2\phi)}{36\phi^2(1 - \phi)^2}\right]\phi'^2 , \tag{4.1}$$

where the dashes denote derivatives with respect to x. The resulting chemical potential profile is shown in Figure 4.3a.

(a)   (b)
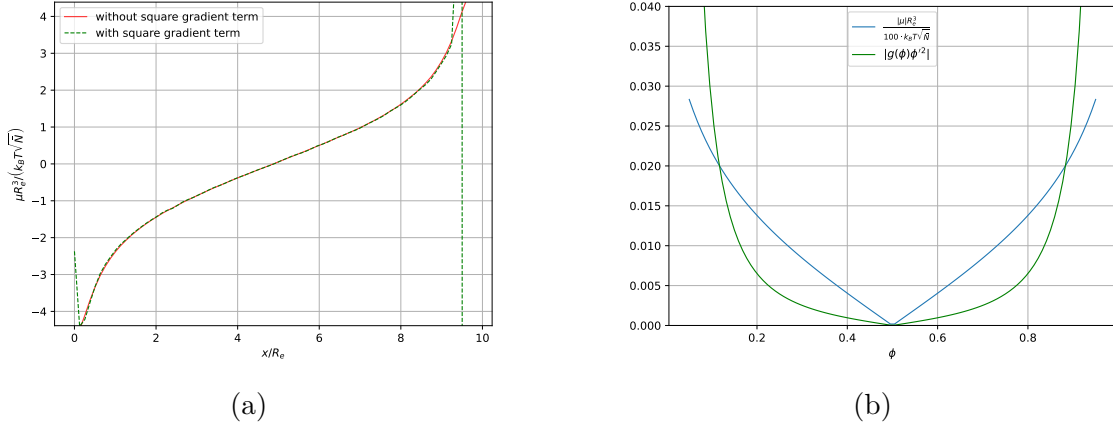
Figure 4.3: (a) Steady-state chemical potential profile obtained from (4.1) for $r = 1.0$, averaged over y and z. (b) $g(\phi)\phi'^2 \equiv R_e^2(1 - 2\phi)\phi'^2/[36\phi^2(1 - \phi)^2]$ and absolute value of chemical potential $|\mu|R_e^3/(100 \cdot k_B T\sqrt{\bar{N}})$. In the discussed case, $\phi' \approx 0.1$.

Evidently, the contribution of the terms involving spatial derivatives of the density to the total chemical potential is negligible, except in a very small region close to the walls. The linearity of the density profile already implies $\phi'' = 0$ and Figure 4.3 shows that the term proportional to ϕ'^2 accounts for less than one percent of the total chemical potential for $0.12 \lesssim \phi \lesssim 0.88$, which roughly corresponds to the region in Figure 4.2 that is assumed to be unaffected by boundary effects. In the subsequent discussion, the terms in (4.1) containing spatial derivatives of ϕ will be neglected. This approximation improves further as the simulation box becomes infinitely long and $\phi' \to 0$. However, for more complex density profiles, the contribution is of course not negligible.

With (2.13) and (4.1), neglecting the terms arising from the square gradient, the current becomes:

$$J = -D\sqrt{\bar{N}}R_e^{-3}\phi' \,, \tag{4.2}$$

Together with (2.10), this gives the standard diffusion equation:

$$\frac{\partial \phi(\mathbf{r},t)}{\partial t} - D\sqrt{\bar{N}}R_e^{-3}\phi'' = 0 \,. \tag{4.3}$$

In the steady state, this simply yields $\phi'' = 0$, so a linear density profile is obtained, as expected. From (4.2) and the condition that $\phi(L_x/2) = 1/2$, which follows from the symmetry of the conversion rates, the density profile becomes:

$$\phi(x) = \frac{JR_e^3}{D\sqrt{\bar{N}}}\left(\frac{L_x}{2} - x\right) + \frac{1}{2} \,. \tag{4.4}$$

To verify (2.17), the Onsager coefficient may also be obtained directly from the simulation results using (2.13). Again assuming local coupling and making use of (4.1), while neglecting the terms arising from the square gradient, one obtains:

$$\Lambda = -\frac{JR_e^3}{\sqrt{\bar{N}}\phi'}\phi(1-\phi). \tag{4.5}$$

The resulting Onsager coefficient is plotted in Figure 4.4.

The Onsager coefficients obtained from (2.17) and (4.5) are in excellent agreement, which hints that the theoretical derivations are consistent with the simulation results. Specifically, the assumptions of incompressibility and local coupling of the current to the chemical potential are justified and the linear density profile observed in Figure 4.2 is explained.
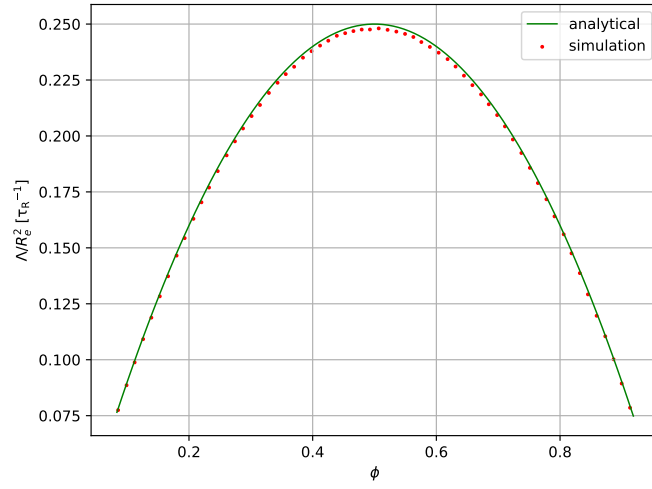
Figure 4.4: Onsager coefficient Λ as a function of ϕ. The analytical curve is obtained from (2.17) and (4.4), the numerical curve from (4.5) and the density profile in 4.2, where ϕ' is obtained from a linear fit. Only data points measured at a distance greater than R_e from the walls are used. The diffusion constant D and the current J are both obtained from the simulation.

5 Outlook

The collective diffusion coefficient of a symmetric homopolymer mixture under a boundary-driven diffusion flux has been studied. In the future, more sophisticated and time-dependent boundary conditions will be employed to manipulate the behavior of the bulk, with the ultimate goal of simulating smaller sections of a large continuum simulation using particle-based simulations. The key question is whether or not the time evolution of the boundary densities is sufficient to dictate the time-evolution of the densities in the bulk. An approach based purely on center-of-mass-based polymer conversion zones might be problematic due to the extension of the converted chains beyond the boundaries. Simple conversions without changing the position of the beads may also lead to unlikely configurations of the affected polymer, so it might be necessary to let the chain grow into the simulation box, e.g. using the configurational bias method [22].

Bibliography

[1] J. Baschnagel, H. Meyer, F. Varnik, S. Metzger, M. Aichele, M. Müller, and K. Binder. Computer simulations of polymers close to solid interfaces: Some selected topics. *Interface Science*, 11(2):159–173, 2003. doi: 10.1023/A: 1022118610890. URL `https://doi.org/10.1023/A:1022118610890`.

[2] Frank S. Bates, Wayne W. Maurer, Paul M. Lipic, Marc A. Hillmyer, Kristoffer Almdal, Kell Mortensen, Glenn H. Fredrickson, and Timothy P. Lodge. Polymeric bicontinuous microemulsions. *Phys. Rev. Lett.*, 79:849–852, Aug 1997. doi: 10.1103/PhysRevLett.79.849. URL `https://link.aps.org/doi/10.1103/PhysRevLett.79.849`.

[3] K. Binder. Collective diffusion, nucleation, and spinodal decomposition in polymer mixtures. *The Journal of Chemical Physics*, 79(12):6387–6409, 1983. doi: 10.1063/1.445747. URL `https://doi.org/10.1063/1.445747`.

[4] Kostas Ch. Daoulas and Marcus Müller. Single chain in mean field simulations: Quasi-instantaneous field approximation and quantitative comparison with monte carlo simulations. *The Journal of Chemical Physics*, 125(18):184904, 2006. doi: 10.1063/1.2364506. URL `https://doi.org/10.1063/1.2364506`.

[5] P. G. de Gennes. Dynamics of fluctuations and spinodal decomposition in polymer blends. *The Journal of Chemical Physics*, 72(9):4756–4763, 1980. doi: 10.1063/1.439809. URL `https://doi.org/10.1063/1.439809`.

[6] Oliver Dreyer, Gregor Ibbeken, Ludwig Schneider, Niklas Blagojevic, Maryam Radjabian, Volker Abetz, and Marcus Müller. Simulation of solvent evaporation from a diblock copolymer film: Orientation of the cylindrical mesophase. *Macromolecules*, 55(17):7564–7582, 2022. doi: 10.1021/acs.macromol.2c00612. URL `https://doi.org/10.1021/acs.macromol.2c00612`.

[7] Dominik Düchs, Venkat Ganesan, Glenn H. Fredrickson, and Friederike Schmid. Fluctuation effects in ternary ab + a + b polymeric emulsions. *Macromolecules*,

36(24):9237–9248, 12 2003. doi: 10.1021/ma030201y. URL `https://doi.org/10.1021/ma030201y`.

[8] I Ya Erukhimovich and AN Semenov. Nonexponential density relaxation and the dynamic form-factor of polymer melts in the reptation regime. *Zh. Eksp. Teor. Fiz*, 63:275, 1986.

[9] Paul J. Flory. Thermodynamics of high polymer solutions. *The Journal of Chemical Physics*, 10(1):51–61, 1942. doi: 10.1063/1.1723621. URL `https://doi.org/10.1063/1.1723621`.

[10] J. G. E. M. Fraaije, B. A. C. van Vlimmeren, N. M. Maurits, M. Postma, O. A. Evers, C. Hoffmann, P. Altevogt, and G. Goldbeck-Wood. The dynamic mean-field density functional method and its application to the mesoscopic dynamics of quenched block copolymer melts. *The Journal of Chemical Physics*, 106(10): 4260–4269, 1997. doi: 10.1063/1.473129. URL `https://doi.org/10.1063/1.473129`.

[11] Ludwik Leibler. Theory of microphase separation in block copolymers. *Macromolecules*, 13(6):1602–1617, 1980.

[12] R.H. Colby M. Rubinstein. *Polymer Physics*. Oxford University Press, 2003.

[13] M. Müller and G. Gompper. Elastic properties of polymer interfaces: Aggregation of pure diblock, mixed diblock, and triblock copolymers. *Phys. Rev. E*, 66:041805, Oct 2002. doi: 10.1103/PhysRevE.66.041805. URL `https://link.aps.org/doi/10.1103/PhysRevE.66.041805`.

[14] Marcus Müller. Studying amphiphilic self-assembly with soft coarse-grained models. *Journal of Statistical Physics*, 145:967–1016, 11 2011. doi: 10.1007/s10955-011-0302-z.

[15] C. Pangali, M. Rao, and B.J. Berne. On a novel monte carlo scheme for simulating water and aqueous solutions. *Chemical Physics Letters*, 55(3): 413–417, 1978. ISSN 0009-2614. doi: https://doi.org/10.1016/0009-2614(78) 84003-2. URL `https://www.sciencedirect.com/science/article/pii/0009261478840032`.

[16] Shuanhu Qi and Friederike Schmid. Hybrid particle-continuum simulations coupling brownian dynamics and local dynamic density functional theory. *Soft*

Matter, 13:7938–7947, 2017. doi: 10.1039/C7SM01749A. URL `http://dx.doi.org/10.1039/C7SM01749A`.

[17] Ellen Reister. *Zusammenhang zwischen der Einzelkettendynamik und der Dynamik von Konzentrationsfluktuationen in mehrkomponentigen Polymersystemen.* PhD thesis, Mainz, 2002.

[18] Peter J. Rossky, Jimmie D. Doll, and Harold L. Friedman. Brownian dynamics as smart monte carlo simulation. *Journal of Chemical Physics*, 69:4628–4633, 1978.

[19] Prince E. Rouse. A theory of the linear viscoelastic properties of dilute solutions of coiling polymers. *The Journal of Chemical Physics*, 21(7):1272–1280, 1953. doi: 10.1063/1.1699180. URL `https://doi.org/10.1063/1.1699180`.

[20] Ludwig Schneider and Marcus Müller. Multi-Architecture Monte-Carlo (MC) Simulation of Soft Coarse-Grained Polymeric Materials: SOft coarse grained Monte-carlo Acceleration (SOMA). *arXiv e-prints*, art. arXiv:1711.03828, November 2017. doi: 10.48550/arXiv.1711.03828.

[21] A. N. Semenov. Theory of Long-Range Interactions in Polymer Systems. *J. Phys. II*, 6(12):1759–1780, December 1996. ISSN 1155-4312. doi: 10.1051/jp2: 1996159.

[22] Jörn Ilja Siepmann and Daan Frenkel. Configurational bias monte carlo: a new sampling scheme for flexible chains. *Molecular Physics*, 75(1):59–70, 1992. doi: 10.1080/00268979200100061. URL `https://doi.org/10.1080/00268979200100061`.

[23] Glenn M. Torrie and John P. Valleau. Monte carlo free energy estimates using non-boltzmann sampling: Application to the sub-critical lennard-jones fluid. *Chemical Physics Letters*, 28(4):578–581, 1974. ISSN 0009-2614. doi: https://doi.org/10.1016/0009-2614(74)80109-0. URL `https://www.sciencedirect.com/science/article/pii/0009261474801090`.